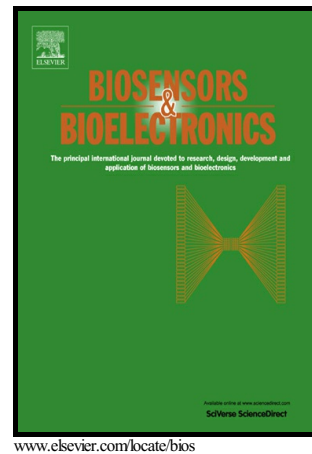# Author's Accepted Manuscript

Metallic-semiconducting junctions create sensing hot-spots in carbon nanotube FET aptasensors near percolation

Murugathas Thanihaichelvan, Leo A. Browning, Marissa P. Dierkes, Roger Martinez Reyes, Andrew V. Kralicek, Colm Carraher, Colleen A. Marlow, Natalie O.V. Plank

Cite this article as: Murugathas Thanihaichelvan, Leo A. Browning, Marissa P. Dierkes, Roger Martinez Reyes, Andrew V. Kralicek, Colm Carraher, Colleen A. Marlow and Natalie O.V. Plank, Metallic-semiconducting junctions create sensing hot-spots in carbon nanotube FET aptasensors near percolation, *Biosensors and Bioelectronic,* https://doi.org/10.1016/j.bios.2018.09.021

Metallic-semiconducting junctions create sensing hot-spots in carbon nanotube FET aptasensors near percolation

Murugathas Thanihaichelvan[a,b,c], Leo A. Browning[a,b], Marissa P. Dierkes[d], Roger Martinez Reyes[d], Andrew V. Kralicek[e], Colm Carraher[e], Colleen A. Marlow[d], Natalie O. V. Plank[a,b*]

[a]School of Chemical and Physical Sciences, Victoria University of Wellington, Wellington 6021, New Zealand.

[b]The MacDiarmid Institute for Advanced Materials and Nanotechnology.

[c]Department of Physics, University of Jaffna, Jaffna 40000, Sri Lanka.

[d]Physics Department, California Polytechnic State University, San Luis Obispo, California, 93407, United States of America.

[e]The New Zealand Institute for Plant & Food Research Limited, Auckland 1142, New Zealand.

*Corresponding author: Address: Victoria University of Wellington, Room 503, Laby Bldg, Kelburn Pde, Wellington 6140, New Zealand. Phone: +6444635031. Email: natalie.plank@vuw.ac.nz

Abstract

Easily fabricated random network carbon nanotube field-effect transistors (CNT-FETs) have benefitted from improved separation techniques to deliver CNTs with current formulations providing at least 99% semiconducting tube content. Amongst the most promising applications of this device platform are electronic biosensors, where the network conduction is affected through tethered probes such as aptamers which act as molecular scale electrostatic gates. However, the prevailing assumption that these biosensor devices would be optimized if metallic tubes were entirely eliminated has not been examined. Here, we show that metallic-semiconducting junctions in aptasensors are sensing hotspots and that their impact on sensing is heightened by the CNT network's proximity to percolation. First, we use a biased conducting AFM tip to gate a CNT-FET at the nanoscale and demonstrate that the strongest device response occurs when gating at metallic-semiconducting junctions. Second, we resolve the target sensitivity of an aptasensor as a function of tube density and show heightened sensitivity at densities close to the percolation threshold. We find the strongest sensing response where the 1% of metallic tubes generate a high density of metallic-semiconducting junctions but cannot form a percolated metallic path across the network. These findings highlight the critical role of metallic tubes in CNT-FET biosensor devices and demonstrate that network composition is an important variable to boost the performance of electronic biosensors.

Keywords: CNT network, FET, Electrostatic gating, Aptasensor, Percolation

1. Introduction

Carbon nanotube field effect transistor (CNT-FET) aptasensors have shown excellent performance for the selective detection of a range of analytes including single proteins, (Hu et al., 2011; Ishikawa et al., 2010; Khosravi et al., 2017; Maehashi et al., 2007; Maehashi and Matsumoto, 2009; Pacios et al., 2012; So et al., 2005) hormones,(Zheng et al., 2015) and metal ions (Zheng et al., 2016) with detection limits on the order of femtomolar concentrations. FETs using both single CNT channel devices (Ordinario et al., 2014; So et al., 2005) and CNT networks (Hu et al., 2011; Ishikawa et al., 2010; Khosravi et al., 2017; Star et al., 2006; Zheng et al., 2016, 2015) have been demonstrated. However, there are advantages around the ease of fabrication for network CNT-FETs where solution processing routes are utilized (Kim et al., 2011; LeMieux et al., 2009, 2008; Opatkiewicz et al., 2012; Park et al., 2016; Rouhi et al., 2011; Son et al., 2017, 2016; Zheng and Plank, 2017). In addition, network CNT-FETs have better device to device reproducibility compared to single carbon nanotube sensors (LeMieux et al., 2008; Rouhi et al., 2011). While network CNT-FET aptasensors have great promise for broad application in bio-sensing, a central challenge to the optimization of these devices is understanding the role that the network morphology plays in their electrical sensitivity to analyte detection. Specifically, while improved tube separation methods can now deliver >99% semiconducting tube content and vastly improved FET characteristics, it is not clear whether the elimination of metallic tubes will lead to improved biosensor devices.

Here we investigate the effects of CNT-CNT junctions in network CNT-FET aptasensors. The active layer of our CNT-FET aptasensors is formed by a thin film random network of 99% semiconducting (s) CNTs (IsoNanotubesS-99) connected by inter-tube junctions (Zheng et al., 2016, 2015). The network consists predominantly of

CNT bundles with some individual CNTs. The small number of metallic (m) tubes and semiconducting tubes of different bandgap (s') than the principal s-CNT lead to the formation of m-s junctions and s-s' junctions in the network in addition to m-m and s-s connections. Previous work on CNT network conduction has shown that energetic barriers form at the m-s and s-s' junctions leading to areas of increased resistance in the network (Fuhrer et al., 2000; Hecht et al., 2006; Lee et al., 2009; Nirmalraj et al., 2009; Rother et al., 2016; Stadermann et al., 2004; Tombler et al., 2000; Topinka et al., 2009). Asymmetric Schottky barriers form at the m-s tube junctions and a heterojunction barrier forms at s-s' junctions due to the bandgap mismatch (Fuhrer et al., 2000). The presence of multi-tube bundle junctions creates bundle-bundle junctions, which restrict conduction less than single tube junctions, since they consist of several tube-tube junctions in parallel. The overall network conductance decreases as both the presence of bundles increases and if larger diameter bundles occur in the network which in both cases has the effect of creating more paths for conduction (Garrett et al., 2010; Hecht et al., 2006; Lamberti et al., 2014; Lyons et al., 2008; Nirmalraj et al., 2009).

In addition to the m-s and s-s' junctions dominating the overall fixed conductance of a CNT network, they play a key role in the dynamic electrical response of the network that occurs during sensing. A recent comprehensive study of CNT-FET gas sensors in which the active layer is a thin film network of CNTs demonstrated that the sensing response of the CNT-FET was dominated by the inter-tube junctions rather than within tube or tube-electrode effects (Boyd et al., 2014). It is therefore important to determine the nature of these junctions; specifically why and how these junctions dominate the network's conductive response.

Here, we show that the presence of high resistance junctions (e.g. m-s and s-s' junctions) alone is not the only factor affecting the overall CNT-FET dynamic sensitivity. The proximity of the network to the critical density for percolation is also important. As previously reported, the mechanism for CNT-FET potassium aptasensing is the electrostatic gating of the CNT network due to conformal changes to the aptamer during the sensing event (Zheng et al., 2016). To simulate this mechanism we use a biased conductive atomic force microscope (c-AFM) tip to electrostatically gate a nanoscopic region of the network while measuring the network's conductive response. We observe that not all junctions, when gated, significantly affect the network conductance. Our combined results strongly indicate that the m-s and s-s' junctions within the network are the dominant source of CNT-FET aptasensor sensitivity, and that network morphology and proximity to percolation can heighten this sensitivity. Therefore maximizing the number of m-s junctions while remaining near the percolation threshold will give maximum sensitivity to a CNT-FET aptasensor.

2. Experimental Methods

2.1. Carbon nanotube network fabrication

CNT thin films were fabricated via a solution deposition process directly onto a flexible Kapton substrate (Kapton 500 HN film, Lohmann). Kapton was selected to avoid the unwanted signal during sensing due to the interaction between potassium ions and dangling bonds on the SiO_2 surface. CNT bucky paper with 99% semiconducting CNTs (Nanointegris, IsoNanotubes S-99) was weighed with a precision balance (Sartorius ME36S), to create a 5 µg/ml CNT suspension in anhydrous 1,2-dichlorobenzene (DCB) (99% Sigma Aldrich) via ultrasonication for

15 min. A cured polydimethylsiloxane (PDMS) (Sylgard 184) surface was cleaned with a 50 W oxygen plasma for 1 min. Next, 10 mg of 2-mercaptopyridine (99%, Sigma Aldrich) was dissolved in 1 ml of ethanol then spin coated onto the PDMS at 2000 rpm for 40 sec. We placed the cleaned Kapton substrates on the 2-mercaptopyridine coated PDMS surface for 3 min to functionalize the Kapton surface (Plank et al., 2005). The substrates were then immersed into the CNT-DCB suspension and the CNT bundle density was varied by regulating the immersion time for 10, 20, 40 or 80 min. Samples were then removed from the suspension and dipped into ethanol for 10 min and dried in nitrogen.

2.2. CNT-FET fabrication

CNT-FETs with channel dimension of 40 μm length and 100 μm width were fabricated using standard microfabrication techniques (Zheng and Plank, 2017). The unwanted CNTs on the substrates were etched with a 200 W oxygen plasma at 600 mTorr for 3 min (Oxford instruments, Plasmalab 80 Plus) (Zheng and Plank, 2017). The source and drain electrodes 5/50 nm chromium/gold were deposited via thermal evaporation (Angstrom engineering – Nex Dep200). The channel of each device was then imaged by atomic force microscopy (Nanosurf, NaioAFM). The source and drain electrodes were then encapsulated by a layer of photoresist AZ1518 (Microchemicals) hard baked at 200°C for 10 min resulting in a channel area 10 μm long and 100 μm wide open to the environment.

2.3. Electrostatic gating of individual junctions on nanoscale

We used the CNT-FET devices fabricated on a 300 nm SiO_2 coated Si substrate (Silicon Quest International, Inc.) to perform AFM gating measurements due to its superior surface roughness and mechanical stability. Nanoscale electrostatic gating

was carried out using a conductive AFM tip as the localized gate. This method is similar to scanning gate microscopy (SGM), however, we did not scan the position of the tip across the network. Instead we held it stationary and swept the bias voltage. The tip was insulated from the network surface with a thin layer of air. A custom electronic device stage allowed for electrical contact to the CNT-FET source and drain electrodes while the device was in the AFM system (Park-XE70). First the AFM was operated in imaging mode to image the network and identify a particular junction within a percolated path then the c-AFM tip was held at the planar location of the junction and then raised to a fixed height above the surface of the CNT network. In this configuration, the network current I_{ds} was measured for a fixed drain source voltage $V_{ds} = 5$ V) as the bias voltage V_{tip} applied to the c-AFM tip was varied.

2.4. Aptamer functionalisation

To functionalize the CNT-FETs for potassium sensing, potassium aptamers were immobilized onto the CNTs in the device channel in a two-stage process. Initially the CNT-FETs were submerged in 1 mM 1-pyrenebutanoicacid, succinimidyl ester (PBASE) (95%, Sigma Aldrich) in methanol for one hour (Kim et al., 2008). The CNT-FETs were washed three times in methanol and then dipped into DI water for 5 s. In parallel the potassium aptamer with sequence of 5′-NH$_2$-TTTGGTTGGTGTGGTTGGTTT-3′ (AlphaDNA, USA) was made into a stock solution of 74 µM in DI (18.2 MΩ) water and stored at -20°C. Prior to attachment to the CNTs a 1 µM aptamer solution in 20 mM tris buffer (pH 7.4) was prepared from the 74 µM stock solution and denatured via heating in an oven for 5 min at 70°C (Alsager et al., 2015, 2014). The PBASE functionalized CNTs were then submerged in the aptamer solution for 2 hrs. The CNT-FETs were then washed three times each in

20 mM tris buffer (pH 7.4) and DI water. A schematic of this functionalisation scheme is shown in Figure S1.

2.5. Device characterization techniques

Electrical sensor measurements were carried out using top liquid gate morphology as shown in the schematic in Figure 1. A PDMS well was used to constrain the electrolyte to the channel region. CNT-FETs were electrically characterized using an Agilent 4156C parameter analyser and a Rucker and Kolls probestation. Ag/AgCl electrodes (BASi, MF2052) were used as the gate electrode for liquid gate measurements.
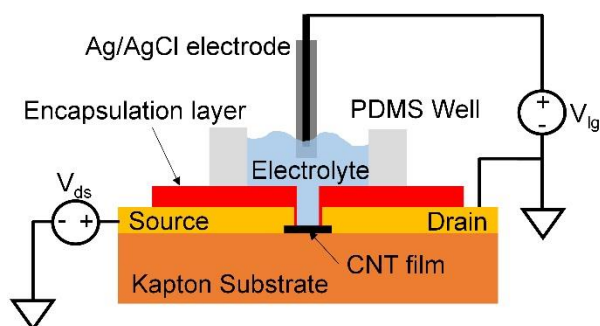

Figure 1. Device schematic of the network CNT-FET fabricated on Kapton substrate with encapsulated source and drain electrodes for liquid gate measurements.

The PDMS well was filled with 100 µl of 2 mM tris buffer (pH 7.4) and the Ag/AgCl electrode was then placed into the buffer. The transfer characteristics of the CNT-FETs were measured at $V_{ds} = 100$ mV while the liquid gate voltage V_{lg} was swept from -0.5 V to 1 V with an interval of 20 mV. The potassium ion solution was prepared with concentrations of 100 pM, 1 nM, 10 nM, 100 nM, 1 µM and 10 µM by dissolving KCl in 2 mM tris (pH 7.4) buffer. The potassium ion solution was added to the well at

intervals of 10 min to vary the solution concentration range from 10 pM to 1 μM. During the potassium sensing V_{lg} was held at 0 V and a constant $V_{ds} = 100$ mV was applied while I_{ds} was measured at 1 sec intervals as the potassium ion solution was introduced.

3. Results and Discussion
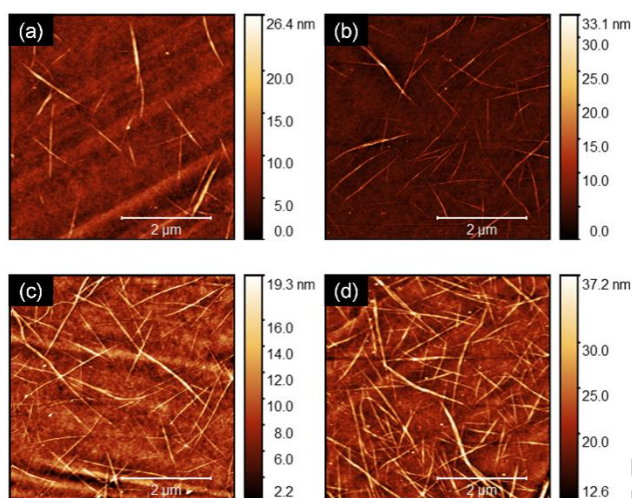
3.1. CNT network morphology

Figure 2. AFM images of CNT films deposited on Kapton substrate with deposition times of (a) 10, (b) 20, (c) 40 and (d) 80 min.

The CNT network morphology was characterized using AFM imaging. Figure 2 shows typical morphology for the deposition times of 10, 20, 40 and 80 min. All of the networks were predominantly composed of multi-tube bundles of varying diameter, consistent with previous work (Khosravi et al., 2017; Lee et al., 2011; Zheng et al., 2016). The AFM images were used to determine the distribution of bundle sizes, bundle density and bundle junctions; see sections 1, 2 and 3 in Thanihaichelvan et al., (2018) for more details. Bundle diameters range from 3-21 nm with a mean value of 8 nm across all deposition times. NanoIntegris specifications state that the CNT diameters are in the range of 1.2-1.7 nm. Using an average diameter of 1.5 nm for an

individual CNT and 2D packing of tubes (Graham et al., 1998) we calculate the number of individual CNTs in each cylindrical bundle (Thanihaichelvan et al., 2018). We obtain an estimate of the percentage of metallic tubes within a bundle of a given diameter by calculating the probability that that bundle will contain at least one metallic tube. The calculation was done for each bundle diameter counted in the observed distribution of bundle sizes and used to determine a 24.09 (±0.85)% probability that any given bundle in the network contains one or more metallic CNT which we deem to be a metallic bundle (Thanihaichelvan et al., 2018). Notably the presence of bundles in our networks significantly increases the presence of metallic elements beyond the 1% metallic tube composition of the original CNT buckypaper that would be present in the absence of bundles (Shimizu et al., 2013).
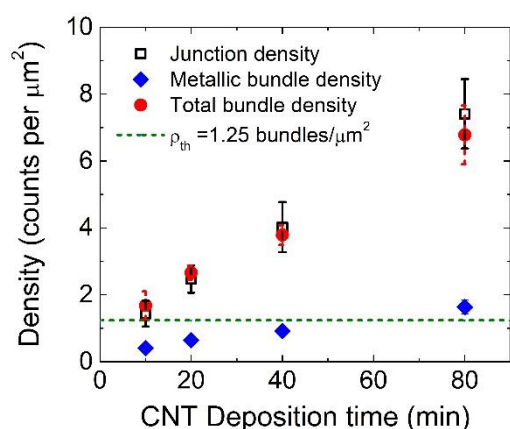

Figure 3. Variation of CNT junction, total bundle density and metallic bundle density as a function of the CNT deposition time. The dashed green line indicates the percolation threshold density of 1.25 bundles/μm^2 for an average bundle length of 2.14 μm.

Network morphology was further characterized by determining the CNT bundle length, junction density and bundle density from the AFM images. Figure 3 shows that

within the range of CNT deposition times both the junction and total bundle density depend linearly on deposition time, indicating that our fabrication method can tune a CNT network's density close to percolation. Each of the data points in Figure 3 is an averaged value calculated from nine images for each of three samples with the same deposition time. Modelling our CNT films using the standard 2D random stick percolation model, the CNT bundle density at percolation threshold (ρ_{th}) can be written as

$$\rho_{th} = 4.236^2/\pi L^2$$

where *L* is the average bundle length (Hu et al., 2004; Kumar et al., 2005; Pike and Seager, 1974; Snow et al., 2003). The average CNT bundle length for our films was 2.14±0.45 µm across all deposition times and predicts a percolation threshold density of 1.25±0.57 bundles/µm^2 which is just below the total bundle density observed for networks with 10 min CNT deposition time (1.43±0.38 bundles/µm^2). The metallic bundles can be thought of as a second network for the purpose of interpreting the electrical properties of the device, shown in Figure 3. When the metallic bundle density is above the percolation threshold an exclusively metallic percolated path exists across the device in parallel with paths of mixed bundle composition.

All CNT-FETs were characterized electrically under a liquid gate, as shown schematically in Figure 1 and described in the Methods section. The transfer characteristics and a summary of the on/off currents, on/off ratios and the threshold voltages for the CNT-FETs are shown in Figure 5 of ref. (Thanihaichelvan et al., 2018) and their transfer characteristics with gate current in Figure 6 of ref. (Thanihaichelvan et al., 2018). Of the CNT-FETs with deposition times of 10 min 41% had an operational CNT film active layer, while for 20 min, 40 min and 80 min deposition times obtained yields of 92%, 100% and 100% respectively. The CNT-

11

FETs exhibit ambipolarity which is consistent with previously reported network CNT-FETs (Derenskyi et al., 2014; Yu et al., 2009). For the CNT-FETs closest to the percolation threshold (deposition times of 10 min) we see larger variation in the on and off currents as expected due to the proximity of those networks to the percolation threshold. As CNT deposition time increases we see an increase in the off current. This is because as the bundle density is increased the network nears the metallic percolation threshold, increasing the likelihood of continuous metallic segments in the network (LeMieux et al., 2008; Rouhi et al., 2011). The combined results in Figure 5 of ref. (Thanihaichelvan et al., 2018) show that as the deposition time of the CNTs is increased the CNT-FET performance becomes more homogenous with less sensitivity to the applied gate voltages.

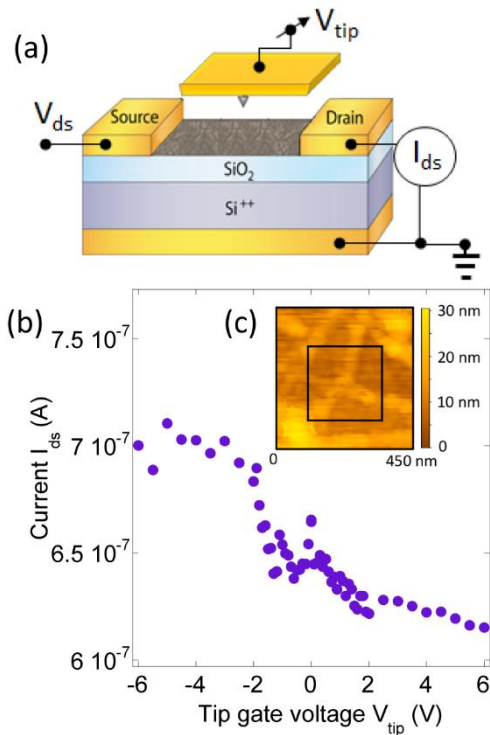*3.2. CNT-FET Response to Gating of Individual Junctions at the Nanoscale*

Figure 4 (a) Schematic of nanoscale gating set-up. (b) Device current (V_{ds} =5 V) with tip bias voltage, V_{tip}, applied to junction showed in inset with a 5 ± 1 nm layer of air

serving as the dielectric. (c) AFM height map of the junction associated with data shown.

To better understand the role of junctions in network CNT-FETs, we used a c-AFM tip as a local gate, similar to SGM (Prisbrey et al., 2012; Tombler et al., 2000; Wilson and Cobden, 2008) to electrostatically affect individual junctions while measuring changes in device current, as shown in Figure 4a. We imaged and gated four individual junctions on two devices, with two junctions on each device. The two devices were fabricated in parallel on the same silicon chip to ensure each device had the same bundle and junction density. These values were determined from AFM images to be 2.02 bundles/μm^2 and 2.14 junctions/μm^2. Figure 4c shows the AFM image of the junction associated with the data in Figure 4b. All four junctions showed no change in device current I_{ds} with applied tip bias V_{tip} for distances between the tip and CNT film surface greater than 6 ± 1 nm. However, one of the four junctions showed a significant change in the network current for a distance of 5 ± 1 nm above the network surface. The tip gate leakage current was less than 1.5 nA in all cases. The conductive response of the network for the case of the junction that did show sensitivity is shown in Figure 4b. As the tip bias was varied from -6 V to +6 V at a fixed distance above the junction the network current was reduced by 100 nA. This decrease in current is consistent with a p-type channel. Our results indicate that the electrostatic gating at the nanometer scale significantly affects the network conductance when the gating occurs near only certain junctions within the network. Wilson and Cobden observed SGM results for CNT networks that show that the network conductance was most sensitive to gating at isolated points in the network rather than along the length of tube segments and does not show sensitivity at all

13

junctions (Wilson and Cobden, 2008). These results are consistent with what we see here.

Previous work demonstrated that m-s junctions and bandgap mismatched s-s' junctions are the most sensitive to electrical changes (Boyd et al., 2014; Lee et al., 2009). We expect that not all junctions in networks of high s-CNT purity should be sensitive to the localized gating of the biased c-AFM, particularly for networks near the percolation threshold density. The *I-V* curves of pristine CNT-FETs, shown in Figure 7 of ref. (Thanihaichelvan et al., 2018), further supports the significance of m-s junction in low density networks. We see that the CNT-FETs fabricated from CNT films deposited at 10 min and 20 min have non-linear characteristics, whereas the CNT-FETs fabricated from CNT films deposited at 40 min and 80 min are linear. The presence of bundles observed in the devices will increase the percentage of m-s junctions present in the network and also increases the likelihood that any individual junction contains at least one bundle rather than two individual CNTs. Since bundle-bundle junctions contain many parallel tube-tube junctions, their presence decreases the effect that an individual tube-tube junction within the bundle-bundle junction has on the transport across the junction. We expect that the junctions that heighten sensitivity are 1) between tubes of mismatched tube types (m-s or s-s') and 2) not contained in a large bundle. Using the AFM image data we can compare the heights of each of the individual junctions locally gated. The measured heights for all four junctions gated were 6.8, 3.1, 10.8 and 8.0 nm. The data shown in Figure 4b is from the junction with a height of 3.1 nm. This value is less than half of the height of the other 3 junctions gated and indicates this junction was made from bundles which contain a single or two CNTs at most. In this case the individual mismatched tube

junction could significantly affect the overall conductance of the network when it is near percolation. Our technique has allowed us to explicitly demonstrate that only certain junctions will dominate the response of the CNT network to local gating on nanometre scales. This has significant implications for the aptasensors that operate via electrostatic gating at molecular length scales (Hu et al., 2011; Khosravi et al., 2017; Zheng et al., 2016, 2015).

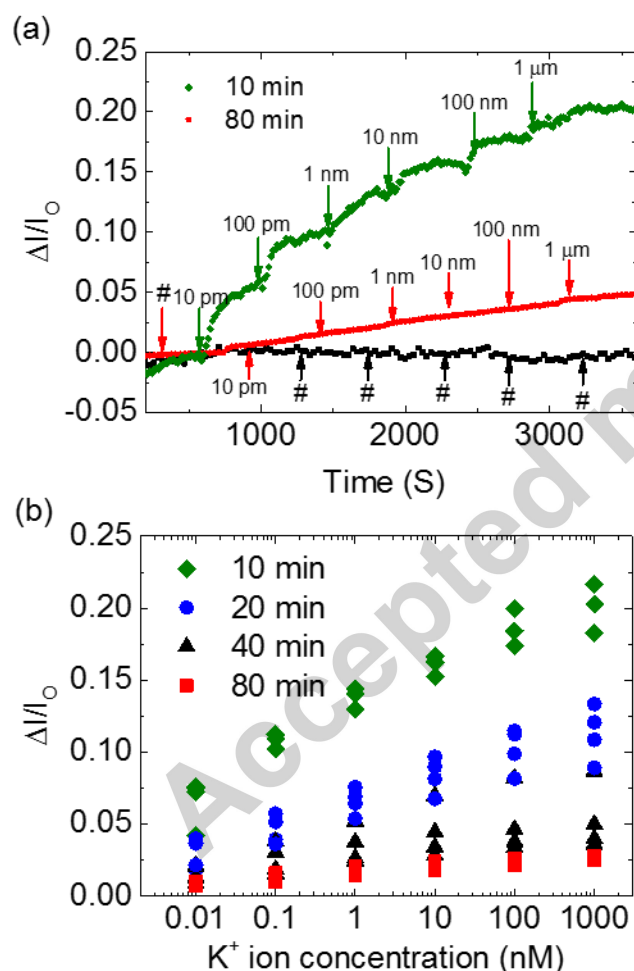### 3.3. CNT-FET Aptasensor Performance

Figure 5. (a) Sensor response of a 10 and 80 min CNT-FET aptasensors measured under liquid gated conditions at $V_{ds} = 100$ mV and liquid gate voltage $V_{lg} = 0$ V. # indicates addition of 10 µl of 2 mM tris buffer (pH 7.4) solution in a 10 min CNT-FET aptasensors. (b) Current

response of liquid gated aptasensors normalized with respect to the zero-potassium concentration I_0 fabricated with CNT networks deposited for 10, 20, 40 and 80 min.

To understand how the role of the junctions in CNT-FET aptasensors is impacted by network morphology we measured the response to potassium exposure as a function of CNT deposition time, shown in Figure 5. Figure S1 illustrates the steps involved in immobilization of aptamers onto CNT sidewalls. The aptasensors with CNT-FET networks closest to percolation showed significantly higher sensitivity to changes in the potassium concentration. Figure 5a shows a typical normalized real time response for a device with a CNT film deposition time of 10 min and 80 min exposed to increasing concentrations of potassium. Potassium addition to the buffer solution (red circles) increases the channel current. In comparison, when an identically prepared sensor is exposed only to the buffer solution over the same intervals the current remains unchanged (black squares). The dependence of the normalized current response of the CNT-FET aptasensors on the CNT deposition time is summarized in Figure 5b. Further validation of our sensors is shown in Figure S2 where we explicitly show the gate current is less than 0.01 nA throughout the sensing process. There is no increase in gate current as K^+ is added to the liquid well, verifying that the increase in current is not due to increased ionic conduction from the K^+ ions.

As shown in table S1, the performance of our 10 min deposition time CNT-FETs are comparable to the best recent CNT network aptasensors. Our results also show CNT-FET aptasensor performance improves with decreasing CNT deposition time with maximum sensitivity for the CNT-FET devices closest to percolation and reduced eight-fold for the deposition time of 80 min. Previous work showed that this structural change to the aptamer during K^+ binding effectively electrostatically gates the CNT

network, shown schematically in Figure S3 in that region which results in increased I_{ds}. (Chen et al., 2013; Huang et al., 2017; Radi and O'Sullivan, 2006; Zheng et al., 2016). Therefore, CNT-FETs with the highest on-off ratios will have the largest current change under electrostatic gating due to the conformal changes of the aptamer in the presence of K^+.
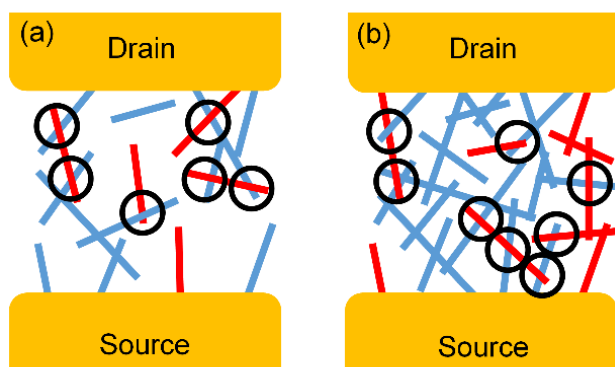
4. Discussion

Figure 6. Schematic of the formation of metal-semiconducting CNT bundle junctions on a (a) sparse and (b) dense CNT network, where the relative densities are comparable to the difference between the 10 min and 80 min CNT-FETs respectively. Bundles with only semiconducting tubes are in blue and those with metallic tubes are in red. The metal-semiconducting junctions are circled.

We propose that the increased sensitivity of the aptasensors with CNT networks close to percolation can be explained in terms of junction density and the total bundle and metallic bundle density presented in Figure 3. Figure 6a and b show schematics of sparse and dense CNT networks, representing films deposited for 10 min and 80 min respectively as calculated from the AFM bundle size data and the likelihood of

17

metallic bundles occurring. Bundles with only semiconducting tubes are blue and bundles containing metallic tubes are red, with the metal-semiconducting junctions circled. The schematic illustrates that for a sparse network near the percolation threshold the conduction will be dominated by a small number of, or even a single, percolated path (Sangwan et al., 2010). Given a 24.09 (±0.85) % chance that bundles contain metallic tubes, these paths will likely have several m-s junctions. With so few, if any, parallel conduction paths these junctions will have a large impact on the current through the entire network (Lee et al., 2009). For CNT-FETs with denser networks as shown in Figure 6b, the increased number of parallel conduction paths diminishes the importance of any given path or individual junction.

For CNT-FETs which are well above percolation but where the metallic bundles are below percolation (e.g. the 40 min CNT deposition time device) there will exist long segments of exclusively metallic bundles which do not span the complete network. While these segments do not provide a percolated path, they allow current to bypass sections of the conduction path containing the higher resistance m-s junctions diminishing their overall impact on the network sensitivity. In contrast, sparse networks in which m-s junctions cannot be avoided transform the m-s junctions into sensing hotspots. It is the combination of the relative composition of metallic tubes along with network morphology and proximity to percolation that allow the mismatched junction sensing hot-spots to have significant impact on current through the network. The sensitivity of these junctions is highly relevant to the aptasensors where the located aptamers directly gate the network at the molecular level.

5. Conclusions

Tuning the electrical properties of CNT-FET platforms is a crucial step in improving the sensitivity of CNT-FET aptamer sensors. We attribute the eight fold increase in the sensitivity of potassium aptasensors, down to 10 pM concentrations, to the increased dominance of key m-s junctions on the conductance of network's close to percolation. We have demonstrated the importance of both the presence of metallic tubes and sparseness of the CNT network in enhancing the sensitivity of CNT-FET aptasensors which detect analytes via an electrostatic gating mechanism. Further investigation into the relative impact of gating effects on m-s junctions and s-s' heterojunctions present in CNT network devices would enhance understanding of the role minority semiconducting CNTs play in CNT-FET aptasensor performance.

Acknowledgements

References

Alsager, O.A., Kumar, S., Willmott, G.R., McNatty, K.P., Hodgkiss, J.M., 2014. Biosens. Bioelectron. 57, 262–268. https://doi.org/10.1016/j.bios.2014.02.004

Alsager, O.A., Kumar, S., Zhu, B., Travas-Sejdic, J., McNatty, K.P., Hodgkiss, J.M., 2015. Anal. Chem. 87, 4201–4209. https://doi.org/10.1021/acs.analchem.5b00335

Boyd, A., Dube, I., Fedorov, G., Paranjape, M., Barbara, P., 2014. Carbon N. Y. 69, 417–423. https://doi.org/10.1016/j.carbon.2013.12.044

Chen, Z., Chen, L., Ma, H., Zhou, T., Li, X., 2013. Biosens. Bioelectron. 48, 108–112. https://doi.org/10.1016/j.bios.2013.04.007

Derenskyi, V., Gomulya, W., Rios, J.M.S., Fritsch, M., Fröhlich, N., Jung, S., Allard, S., Bisri, S.Z., Gordiichuk, P., Herrmann, A., Scherf, U., Loi, M.A., 2014. Adv. Mater. 26, 5969–5975. https://doi.org/10.1002/adma.201401395

Fuhrer, M.S., Nygård, J., Shih, L., Forero, M., Yoon, Y.G., Mazzoni, M.S.C., Choi, H.J., Ihm, J., Louie, S.G., Zettl, A., McEuen, P.L., 2000. Science (80-.). 288, 494–497. https://doi.org/10.1126/science.288.5465.494

Garrett, M.P., Ivanov, I.N., Gerhardt, R.A., Puretzky, A.A., Geohegan, D.B., 2010. Appl. Phys. Lett. 97, 163105. https://doi.org/10.1063/1.3490650

Graham, R.L., Lubachevsky, B.D., Nurmela, K.J., Östergård, P.R.J., 1998. Discrete Math. 181, 139–154. https://doi.org/10.1016/S0012-365X(97)00050-2

Hecht, D., Hu, L., Grüner, G., 2006. Appl. Phys. Lett. 89, 1–4. https://doi.org/10.1063/1.2356999

Hu, L., Hecht, D.S., Gruner, G., Grüner, G., L. Hu, D. S. Hecht, and, Grüner, G., 2004. Nano Lett. 4, 2513–2517. https://doi.org/10.1021/nl048435y

Hu, P., Zhang, J., Wen, Z., Zhang, C., 2011. Nanotechnology 22, 335502. https://doi.org/10.1088/0957-4484/22/33/335502

Huang, J., Su, X., Li, Z., 2017. Biosens. Bioelectron. 96, 127–139. https://doi.org/10.1016/j.bios.2017.04.032

Ishikawa, F.N., Curreli, M., Olson, C.A., Liao, H.I., Sun, R., Roberts, R.W., Cote, R.J., Thompson, M.E., Zhou, C., 2010. ACS Nano 4, 6914–6922. https://doi.org/10.1021/nn101198u

Khosravi, F., Loeian, S.M., Panchapakesan, B., 2017. Biosensors 7.

https://doi.org/10.3390/bios7020017

Kim, J.P., Lee, B.Y., Hong, S., Sim, S.J., 2008. Anal. Biochem. 381, 193–198.

https://doi.org/10.1016/j.ab.2008.06.040

Kim, T.H., Song, H.S., Jin, H.J., Lee, S.H., Namgung, S., Kim, U., Park, T.H., Hong, S.,

2011. Lab Chip 11, 2262. https://doi.org/10.1039/c0lc00648c

Kumar, S., Murthy, J.Y., Alam, M.A., 2005. Phys. Rev. Lett. 95, 66802.

https://doi.org/10.1103/PhysRevLett.95.066802

Lamberti, P., Mousavi, S.A., Spinelli, G., Tucci, V., Wagner, V., 2014. IEEE Trans.

Nanotechnol. 13, 795–804. https://doi.org/10.1109/TNANO.2014.2322284

Lee, B.Y., Sung, M.G., Lee, J., Baik, K.Y., Kwon, Y.K., Lee, M.S., Hong, S., 2011. ACS

Nano 5, 4373–4379. https://doi.org/10.1021/nn103056s

Lee, E.J.H., Balasubramanian, K., Burghard, M., Kern, K., 2009. Adv. Mater. 21, 2720–

2724. https://doi.org/10.1002/adma.200803545

LeMieux, M.C., Roberts, M., Barman, S., Yong, W.J., Jong, M.K., Bao, Z., 2008. Science

(80). 321, 101–104. https://doi.org/10.1126/science.1156588

LeMieux, M.C., Sok, S., Roberts, M.E., Opatkiewicz, J.P., Liu, D., Barman, S.N., Patil, N.,

Mitra, S., Bao, Z., 2009. ACS Nano 3, 4089–4097. https://doi.org/10.1021/nn900827v

Lyons, P.E., De, S., Blighe, F., Nicolosi, V., Pereira, L.F.C., Ferreira, M.S., Coleman, J.N.,

2008. J. Appl. Phys. 104, 44302. https://doi.org/10.1063/1.2968437

Maehashi, K., Katsura, T., Kerman, K., Takamura, Y., Matsumoto, K., Tamiya, E., 2007.

Anal. Chem. 79, 782–787. https://doi.org/10.1021/ac060830g

Maehashi, K., Matsumoto, K., 2009. Sensors 9, 5368–5378.

https://doi.org/10.3390/s90705368

Nirmalraj, P.N., Lyons, P.E., De, S., Coleman, J.N., Boland, J.J., 2009. Nano Lett. 9, 3890–

21

3895. https://doi.org/10.1021/nl9020914

Opatkiewicz, J.P., Lemieux, M.C., Liu, D., Vosgueritchian, M., Barman, S.N., Elkins, C.M., Hedrick, J., Bao, Z., 2012. ACS Nano 6, 4845–4853. https://doi.org/10.1021/nn300124y

Ordinario, D.D., Burke, A.M., Phan, L., Jocson, J.-M., Wang, H., Dickson, M.N., Gorodetsky, A.A., 2014. Anal. Chem. 86, 8628–8633. https://doi.org/10.1021/ac501441d

Pacios, M., Martin-Fernandez, I., Borrisé, X., del Valle, M., Bartrolí, J., Lora-Tamayo, E., Godignon, P., Pérez-Murano, F., Esplandiu, M.J., 2012. Nanoscale 4, 5917. https://doi.org/10.1039/c2nr31257c

Park, M., Kim, S., Kwon, H., Hong, S., Im, S., Ju, S.Y., 2016. ACS Appl. Mater. Interfaces 8, 23270–23280. https://doi.org/10.1021/acsami.6b06932

Pike, G.E., Seager, C.H., 1974. Phys. Rev. B 10, 1421–1434. https://doi.org/10.1103/PhysRevB.10.1421

Plank, N.O. V., Ishida, M., Cheung, R., 2005. J. Vac. Sci. Technol. B Microelectron. Nanom. Struct. 23, 3178. https://doi.org/10.1116/1.2134713

Prisbrey, L., Blank, K., Moshaa, A., Minotl, E.D., 2012. Microsc. Anal. 26, 7–10.

Radi, A.-E., O'Sullivan, C.K., 2006. Chem. Commun. 3432. https://doi.org/10.1039/b606804a

Rother, M., Schießl, S.P., Zakharko, Y., Gannott, F., Zaumseil, J., 2016. ACS Appl. Mater. Interfaces 8, 5571–5579. https://doi.org/10.1021/acsami.6b00074

Rouhi, N., Jain, D., Zand, K., Burke, P.J., 2011. Adv. Mater. 23, 94–99. https://doi.org/10.1002/adma.201003281

Sangwan, V.K., Behnam, A., Ballarotto, V.W., Fuhrer, M.S., Ural, A., Williams, E.D., 2010. Appl. Phys. Lett. 97, 1–4. https://doi.org/10.1063/1.3469930

Shimizu, M., Fujii, S., Tanaka, T., Kataura, H., 2013. J. Phys. Chem. C 117, 11744–11749.

https://doi.org/10.1021/jp3113254

Snow, E.S., Novak, J.P., Campbell, P.M., Park, D., 2003. Appl. Phys. Lett. 82, 2145–2147. https://doi.org/10.1063/1.1564291

So, H.M., Won, K., Kim, Y.H., Kim, B.K., Ryu, B.H., Na, P.S., Kim, H., Lee, J.O., 2005. J. Am. Chem. Soc. 127, 11906–11907. https://doi.org/10.1021/ja053094r

Son, M., Kim, D., Ko, H.J., Hong, S., Park, T.H., 2017. Biosens. Bioelectron. 87, 901–907. https://doi.org/10.1016/j.bios.2016.09.040

Son, M., Kim, D., Park, K.S., Hong, S., Park, T.H., 2016. Biosens. Bioelectron. 78, 87–91. https://doi.org/10.1016/j.bios.2015.11.029

Stadermann, M., Papadakis, S.J., Falvo, M.R., Novak, J., Snow, E., Fu, Q., Liu, J., Fridman, Y., Boland, J.J., Superfine, R., Washburn, S., 2004. Phys. Rev. B - Condens. Matter Mater. Phys. 69, 201402. https://doi.org/10.1103/PhysRevB.69.201402

Star, A., Tu, E., Niemann, J., Gabriel, J.-C.P., Joiner, C.S., Valcke, C., 2006. Proc. Natl. Acad. Sci. 103, 921–926. https://doi.org/10.1073/pnas.0504146103

Thanihaichelvan, M., Browning, L.A., Dierkes, M.P., Reyes, R.M., Kralicek, A. V., Carraher, C., Marlow, C.A., Plank, N.O. V., 2018. Data Br.

Tombler, T.W., Zhou, C., Kong, J., Dai, H., 2000. Appl. Phys. Lett. 76, 2412–2414. https://doi.org/10.1063/1.125611

Topinka, M.A., Rowell, M.W., Goldhaber-Gordon, D., McGehee, M.D., Hecht, D.S., Gruner, G., 2009. Nano Lett. 9, 1866–1871. https://doi.org/10.1021/nl803849e

Wilson, N.R., Cobden, D.H., 2008. Nano Lett. 8, 2161–2165. https://doi.org/10.1021/nl080488i

Yu, W.J., Kim, U.J., Kang, B.R., Lee, I.H., Lee, E.H., Lee, Y.H., 2009. Nano Lett. 9, 1401–1405. https://doi.org/10.1021/nl803066v

Zheng, H.Y., Alsager, O.A., Wood, C.S., Hodgkiss, J.M., Plank, N.O. V., 2015. J. Vac. Sci.

Technol. B, 33, 06F904. https://doi.org/10.1116/1.4935246

Zheng, H.Y., Alsager, O.A., Zhu, B., Travas-Sejdic, J., Hodgkiss, J.M., Plank, N.O. V., 2016. Nanoscale 8, 13659–13668. https://doi.org/10.1039/C5NR08117C

Zheng, H.Y., Plank, N.O.V., 2017. Int. J. Nanotechnol. 14, 505. https://doi.org/10.1504/IJNT.2017.082473

Highlights

- 4 orders of magnitude improvement in the on-off ratios of random network CNT FETs is achieved by varying the CNT network deposition time

- CNT FETs can be fabricated with network densities at, or close to, the percolation threshold

- Key m-s junctions become dominant in the overall CNT FET conduction for sparse networks without parallel conduction paths

- Gate sensitive m-s junctions in the network provide sensing hotspots for aptasensors when electrostatic gating is the dominant sensing mechanism

- 8 fold increase in sensitivity down to 10 pM concentrations of potassium is achieved for potassium aptasensors by tuning the CNT network density close to the percolation threshold